6-1-2005

Target Detection in a Structured Background Environment Using an Infeasibility Metric in an Invariant Space

Emmett J. Ientilucci
Rochester Institute of Technology

John R. Schott
Rochester Institute of Technology

Recommended Citation
Emmett J. Ientilucci, John R. Schott, "Target detection in a structured background environment using an infeasibility metric in an invariant space", Proc. SPIE 5806, Algorithms and Technologies for Multispectral, Hyperspectral, and Ultraspectral Imagery XI, (1 June 2005); doi: 10.1117/12.605850; https://doi.org/10.1117/12.605850

Target Detection in a Structured Background Environment Using an Infeasibility Metric in an Invariant Space

Emmett J. Ientilucci and John R. Schott

Digital Imaging and Remote Sensing Laboratory, Rochester Institute of Technology
54 Lomb Memorial Drive, Rochester, NY 14623-5604

ABSTRACT

This paper develops a hybrid target detector that incorporates structured backgrounds and physics based modeling together with a geometric infeasibility metric. More often than not, detection algorithms are usually applied to atmospherically compensated hyperspectral imagery. Rather than compensate the imagery, we take the opposite approach by using a physics based model to generate permutations of what the target might look like as seen by the sensor in radiance space. The development and status of such a method is presented as applied to the generation of target spaces. The generated target spaces are designed to fully encompass image target pixels while using a limited number of input model parameters.

Background spaces are modeled using a linear subspace (structured) approach characterized by endmembers found by using the maximum distance method (MaxD). After augmenting the image data with the target space, 15 endmembers were found, which were not related to the target (*i.e.,* background endmembers).

A geometric infeasibility metric is developed which enables one to be more selective in rejecting false alarms. Preliminary results in the design of such a metric show that an orthogonal projection operator based on target space vectors can distinguish between target and background pixels. Furthermore, when used in conjunction with an operator that produces abundance-like values, we obtained separation between target, background, and anomalous pixels. This approach was applied to HYDICE image spectrometer data.

Keywords: Hyperspectral, Target Detection, Matched Filter, Infeasibility, Invariant Subspace, Physics Based Modeling

1. INTRODUCTION

This paper investigates a geometric hybrid technique for the detection of subpixel targets in uncompensated image spectrometer data. More often than not, detection algorithms are usually applied to atmospherically compensated hyperspectral imagery. Rather than compensate the imagery, we take the opposite approach by using a physics based model to generate permutations of what the target might look like as seen by the sensor. The physics model predicts what the sensor-reaching radiance looks like based on direct solar illumination, upwelled and downwelled radiances as well as reflectivity of the target. This model is run in an iterative manner with an atmospheric propagation model to produce an illumination invariant (radiance) target space. This paper describes the implementation and status of such a technique.

The approach we take throughout this research is geometric or structured in nature. Therefore, in developing our hybrid detector, we describe the background data using a linear subspace approach characterized by endmembers found using the maximum distance method (MaxD)(*cf.* Sec. 2.3.1). We then present a detector that incorporates a standard orthogonal projection operator that tells us how much influence the background space has on an image pixel. The output of such a detector is an abundance-like term where large values are synonymous with targets. In general, however, the output of the detector may produce large values, not only for actual targets, but for any other spectral anomaly that has a significant projection (*e.g.,* a bright or saturated pixel) thus producing false alarms. Geometrically, we recognize where these cases can occur. We note that there

Further Information:
emmett@cis.rit.edu, Tel: 585-475-7778, Fax: 585-475-5988
schott@cis.rit.edu, Tel: 585-475-5170, Fax: 585-475-5988

Algorithms and Technologies for Multispectral, Hyperspectral, and Ultraspectral Imagery XI,
edited by Sylvia S. Shen, Paul E. Lewis, Proceedings of SPIE Vol. 5806
(SPIE, Bellingham, WA, 2005) · 0277-786X/05/$15 · doi: 10.1117/12.605850

exists many different image pixels that can have the same background influence or abundance. These pixels may manifest themselves as false positives. We separate such pixels through incorporation of an orthogonal projection operator based on a physically derived target space.

Furthermore, we develop the theory for an additional metric that takes advantage of the target and background distributions in such a way that we are able to examine how far a pixel is from the expected target / background mixture. We can then us this additional information to be more selective in rejecting false alarms.

2. THEORY AND APPLICATION

2.1. Physics Based Modeling (PBM)

In target detection, we often seek to atmospherically compensate hyperspectral imagery so as to convert sensor reaching radiance to ground leaving spectral reflectance. Once the imagery has been compensated, detection algorithms are used to compare image reflectances to library or measured reflectances in search of a desired target. Rather than compensate the imagery, an alternative is to estimate what the ground leaving spectral reflectance would look like as seen by the sensor in radiance space.[1] This approach entails modeling the propagation of a target reflectance spectrum through the atmosphere up to the sensor. The advantage this technique has over that of compensated imagery is that target illumination variations can be integrated into the process through use of a physical model thus making the approach *invariant* to illumination effects. Schott[2] derives such a physical model for the spectral radiance reaching an airborne or satellite sensor which incorporates direct illumination variation as well as downwelling and upwelling (or path) radiance. This model can be expressed in simplified form as

$$L_p(\lambda) = \int_\lambda \beta_p(\lambda) \left[\Big(E'_s(\lambda)\tau_1(\lambda)\cos\theta + FE_d(\lambda) \Big)\tau_2(\lambda)\frac{r(\lambda)}{\pi} + L_u(\lambda) \right] \mathrm{d}\lambda \tag{1}$$

where $L_p(\lambda)$ is the effective spectral radiance in the p^{th} band in units of $[Wcm^{-2}sr^{-1}\mu m^{-1}]$, $E'_s(\lambda)$ is the exoatmospheric spectral irradiance from the Sun in units of $[Wcm^{-2}\mu m^{-1}]$, $\tau_1(\lambda)$ is the transmission through the atmosphere along the Sun-target path, θ is the angle from the surface normal to the Sun, F is the fraction of the spectral irradiance from the sky ($E_d(\lambda)$) incident on the target (*i.e.*, not blocked by adjacent objects), $\tau_2(\lambda)$ is the transmission along the target-sensor path, $r(\lambda)$ is the spectral reflectance factor for the target of interest (*i.e.*, $r(\lambda)/\pi$ is the bidirectional reflectance $[sr^{-1}]$), $L_u(\lambda)$ is the spectral path radiance $[Wcm^{-2}sr^{-1}\mu m^{-1}]$, and $\beta_p(\lambda)$ is the normalized spectral response of the p^{th} spectral channel of the sensor under study where

$$\beta_p(\lambda) = \frac{\beta'_p(\lambda)}{\int \beta'_p(\lambda)\,\mathrm{d}\lambda} \tag{2}$$

with $\beta'_p(\lambda)$ being the peak normalized spectral response of the p^{th} channel. Schott[2] also describes how the MODTRAN radiative transfer code[3] can be used to solve for each of the radiometric terms in Eq. (1) (*i.e.*, $E'_s(\lambda), \tau_1(\lambda), \tau_2(\lambda), E_d(\lambda), \text{and } L_u(\lambda)$) given a set of atmospheric and illumination descriptors. Once the terms are solved for, the spectral radiance target vector $\mathbf{x}$ observed by a p-channel sensor can be expressed as

$$\mathbf{x} = [L_1(\lambda), L_2(\lambda), \ldots, L_p(\lambda)]^T. \tag{3}$$

2.2. Generating Target Spaces

In practice, a *family* of radiance vectors is usually generated to account for lack of knowledge about atmospheric, illumination and viewing conditions. This is accomplished by varying the inputs to MODTRAN to span a range of variables. In doing so, a wide range of potential target spectral vectors spanning a *target space* can be generated from a single target reflectance spectrum.

Previous studies[1] have generated such target spaces with over 28,000 spectra in them, 17,000 of which were physically realizable. These target spaces were extensive because of the large number of MODTRAN input parameters varied, particularly the gas concentrations. Atmospheric gas parameters such as O_3, CO,

CO_2, CH_4, N_2O, O_2, were varied along with solar zenith angle, aerosol type, sensor altitude, and water vapor. More recently,[4] however, varied parameters included the MODTRAN atmospheric and aerosol models, visibility, solar zenith angle, and occlusion.

In the earlier method that alters the concentrations of various atmospheric gases, the combinatorial variations between the gasses may not be necessary since the concentrations of these "ideal" gasses should co-vary with each other. By representing the molecular gas species as a single modification in the generation of a look-up-table (LUT), a series of MODTRAN runs that represent improbable conditions can be eliminated from the simulation runs. In the following sections we narrow the number of input parameters to a handful that we believe can adequately characterize the atmosphere and how the target might appear as seen by the sensor. We illustrate these results in Sec. 3.1 where we discuss the creation of both target and background spaces.

2.2.1. Variation in Elevation

The problem with varying each individual constituent parameter, for example, is that we are not taking advantage of actual physical interactions among molecules. Ultimately, by varying the gas parameters, we are after the amount of molecular absorption. Using the "combinations" method will certainly generate physically un-realizable spectra, in addition to unnecessary runs. Since there exists a multitude of dependencies within the atmospheric physical process, a more elegant solution would be to simply vary the *elevation* $[m]$ parameter in MODTRAN which takes into account the fact that gasses co-vary. This parameter controls how much molecular absorption there is in a column of air. Variability in the elevation parameter accounts for the sensor platform altitude, atmospheric pressure, and topography of the ground. If the platform is fairly steady and the ground relatively flat, for example, the variation in the elevation parameter will be small.

2.2.2. Variation in Visibility

In the original implementation of the invariant method,[1] 4 MODTRAN aerosol types were varied. That is, urban, rural, maritime, and desert. For most studies, however, one may be able to choose an aerosol type, based on the given data set. Once selected, we propose to further vary the aerosol *number density* (concentration of number of particles) using the (horizontal) *visibility* $[km]$ parameter in MODTRAN. That is, the number of particles of a certain type that exist in the atmosphere. More recent studies[4] have varied both aerosol type and visibility.

Since this parameter directly impacts atmospheric scattering, it will have a major effect on sensor reaching spectra in the VNIR region (400-1000 nm). An initial estimate of visibility can be obtained from National Oceanic and Atmospheric Administration (NOAA) or a local airport where records of perceived horizontal visibility and general surface weather conditions (including variation), are kept.

2.2.3. Estimation of Water Vapor

Water vapor is by far the largest contributor to absorption in the atmosphere, as can be seen in Figure 1. This constituent directly impacts atmospheric transmission and ultimately sensor-reaching radiance. Water vapor is usually measured as relative humidity (RH), as a function of altitude, and then converted to a measure of precipitable water in g/m^3 or, more commonly, *centimeters* of water in in a given column. Ideally, one would like to have an atmospheric water vapor profile above the target of interest. This can be achieved by launching a radiosonde balloon at the site. This information can then be used as input to MODTRAN so as to generate sensor reaching radiance spectra that reflect the conditions at the time of image acquisition.

In general, it would would behoove us to understand water vapor since it has such a significant impact on sensor-reaching radiance. In the event that radiosonde data is not available, we need to formulate a best guess as to what the atmospheric water content is. If given a specific hyperspectral data set, we can take some of the guess work out of the process by using *physically derived* values of integrated column water vapor obtained through use of estimation algorithms. Each MODTRAN run provides us with an integrated column water vapor value as a function of the input parameters (actual radiosonde or water vapor column scaling factors). From this, we can compare the MODTRAN derived integrated values with those found using estimation algorithms. When can then determine the appropriate water vapor scale factor to use in the MODTRAN run. Variability in the water vapor scalars comes from both the physically derived water map and from historical profiles in and around the surrounding area.

Water Vapor Estimation Algorithms

In cases where measurements are not available or a need to validate the applicability of a given measurement to a site particularly if the measurement site (*e.g.,* airport or weather station) is in a different location than the site of interest, there are in-scene techniques that can yield image derived estimates of water vapor.

The continuum interpolated band removal (CIBR)[5] algorithm is one such program that can be used to estimate water vapor. It is based on looking at the 940 nm absorption feature and relating its depth to water vapor on a per pixel basis. To obtain variability here, one would simple look at the variability in the calculated water vapor map. An improvement to the CIBR model is the atmospheric pre-corrected differential absorption (APDA)[6] algorithm. lt combines a partial atmospheric correction with a differential absorption technique. It works by iteratively correcting for the atmospheric path radiance term leading to the retrieval of water vapor. Again, this process yields per pixel values where variability can be interpreted from the water vapor map. Studies comparing these two methods[7] have shown that they both did a reasonable job of estimating water vapor column abundance.

2.2.4. Variation in Target Orientation

Even if the spectral character of the target, as seen by the sensor through the atmosphere, is modeled correctly in MODTRAN, we still may have issues related to spectral magnitude. This can manifest itself as a time of day (TOD) variation, target-to-sensor angle or orientation variation, or both. The spectra produced by MODTRAN is based on a given TOD and therefore already incorporates attenuation due to the zenith angle (*i.e.,* $\cos\theta$). For this study we vary the orientation of the target relative to the given zenith angle. This can be viewed as *effectively* varying the zenith angle in magnitude only. In past studies, 6 to 8 unique zenith angles were varied.[1,4]

2.2.5. Variation Due to Calibration Errors

A major difference between a target space created using physics-based modeling and one that could be created using image derived targets (in radiance space) is that PBM approach his perfect calibration. That is, there are no sources of error or variability in the space other than from the original reflectance and propagation model which created it. Certainly a target space of this nature fails to resemble real world (target) data to some degree. As a result calibration issues need to be addressed. Given a particular sensor, these sources of error can take on the form of spectrally correlated noise and/or spectral shift or jitter.

2.3. Structured Background Environment

In target detection, there are many methods (and corresponding models) for estimating or describing targets and backgrounds. For example, some methods that describe data in a stochastic sense use parameters such as means and covariances. Still other methods describe the data through use of vector geometry and endmembers. We term these two approaches to data description *unstructured* and *structured*, the latter of which is related to the geometric techniques used in this paper. Most structured approaches use a simple linear mixing model (LMM) to describe pixel content in the imagery. This paper also uses the LMM approach along with a method of finding endmembers called the maximum distance method (MaxD), described in the next section. Ultimately, however, we need to choose a test statistic, the choice of which is driven by the data description type. In this paper we address the geometric approach to detection with the development of a hybrid approach that encompass physics based modeling and an infeasibility metric based on the statistics of the data.

2.3.1. Generating Basis Vectors

A recently developed geometric method for finding endmembers is called is called the maximum distance (MaxD) method.[8,9] This method consists of finding *native* (*i.e.,* vectors that are in the original image space) endmember vectors that best approximate a simplex defining the target or background subspace. The technique starts with identifying two pixels, one with the largest magnitude vector (denoted by $\mathbf{v}_1$) and one with the smallest magnitude (denoted by $\mathbf{v}_2$). Next, all pixel vectors are projected along $\mathbf{v}_1 - \mathbf{v}_2$ onto the subspace orthogonal to $\mathbf{v}_1 - \mathbf{v}_2$ (*cf.* Figure 2a). In this projection, both $\mathbf{v}_1$ and $\mathbf{v}_2$ project on the same point (which we will call $\mathbf{v}_{12}$). Then, the distance between $\mathbf{v}_{12}$ and the remaining projections are calculated. The pixel with the maximum distance to $\mathbf{v}_{12}$ is the third endmember (denoted by $\mathbf{v}_3$). All projected points are now projected along $\mathbf{v}_{12} - \mathbf{v}_3$. The resulting end-member is denoted by $\mathbf{v}_{123}$. The process is repeated until a desired number of endmembers is identified. If

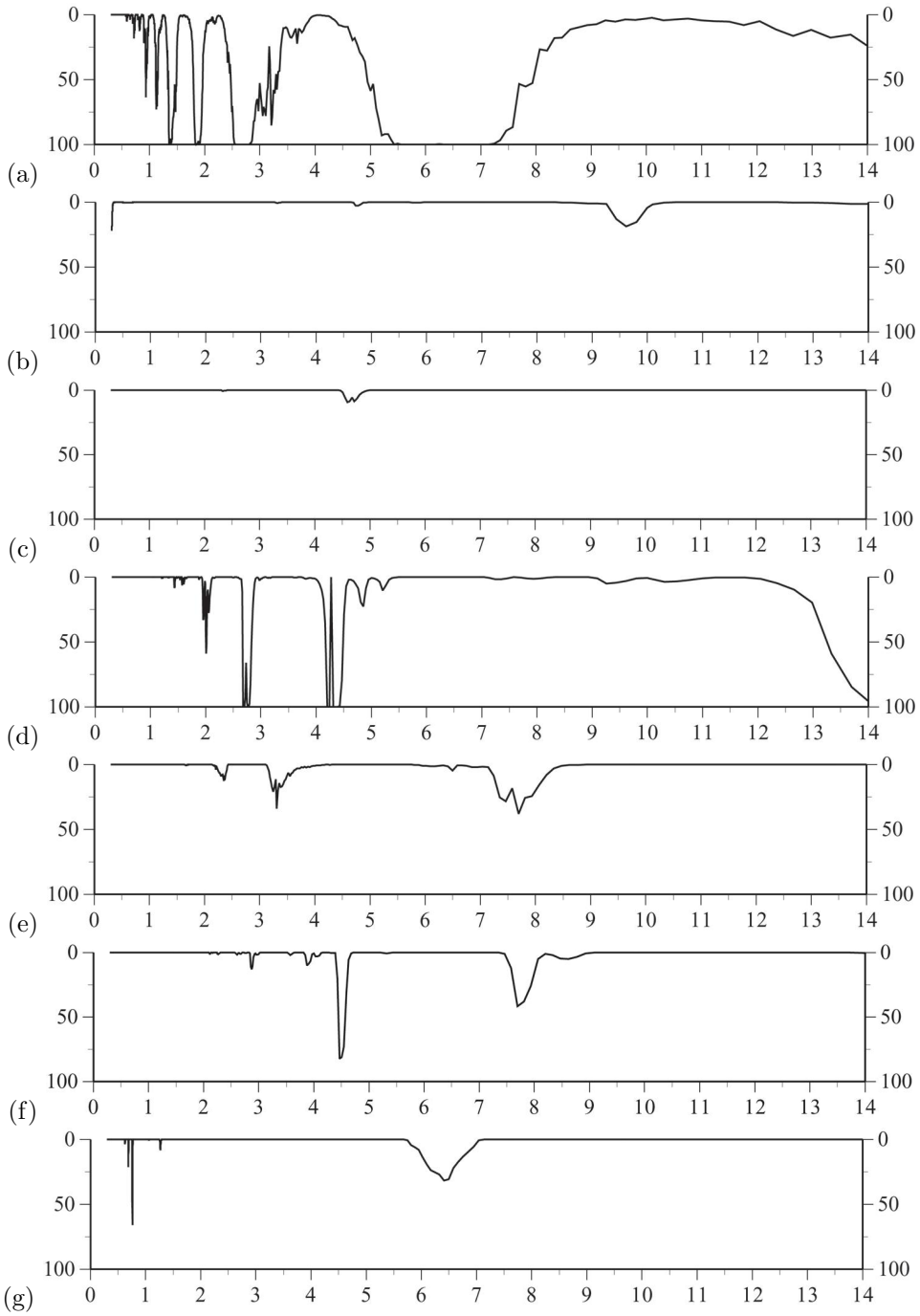

Figure 1. Absorption spectra of (a) H_2O, (b) O_3, (c) CO, (d) CO_2, (e) CH_4, (f) N_2O, and (g) O_2 as a function of wavelength [μm]. We can see that of all the atmospheric constituents, H_2O is the largest contributor to absorption.[2]

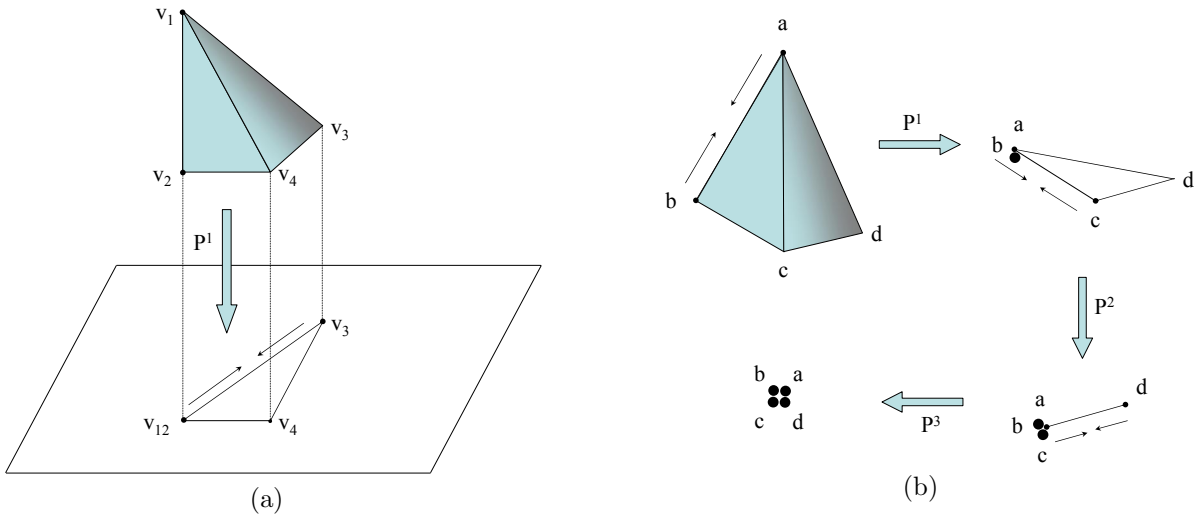

Figure 2. Illustration of (a) the preservation of vertices of a simplex through projection of a data set onto the difference in two vertices of a simplex and (b) the concept of maximum distance determination and sequential projection to find the vertices of a simplex spanning the data space.

this process is continued until $(p+1)$ endmembers are identified, all projected points reduce to one point, and the process can no longer be continued. That is, we can identify up to $(p+1)$ endmembers using MaxD, which is not a limitation in practice when working with hyperspectral images. Additionally, the MaxD method is very fast computationally and is fully automated.

2.4. Structured and Hybrid Target Detection

If the target and backgrounds are described using geometric techniques then the application of a detector based on vector geometry is most appropriate. We first describe the data simplex with a set of endmembers or basis vectors. These endmembers are then used as column vectors to populate a background descriptor matrix, $\mathbf{B}$. We can use this information about the background space to develop a least squares (orthogonal) projection operator that tells us how unlike the background a pixel appears. This non-background-like behavior $\mathbf{e}$ can be described as

$$\mathbf{e} = \mathbf{P}_{\mathbf{B}}^{\perp}\mathbf{x} \tag{4}$$

where the orthogonal projection operator $\mathbf{P}_{\mathbf{B}}^{\perp} = \mathbf{I} - \mathbf{B}\mathbf{B}^{\dagger}$ and $\mathbf{B}^{\dagger}$ is the pseudo-inverse (in a least squares sense) of $\mathbf{B}$ defined as $\mathbf{B}^{\dagger} = (\mathbf{B}^T\mathbf{B})^{-1}\mathbf{B}^T$. The quantity $\mathbf{B}\mathbf{B}^{\dagger}$ is known in matrix theory as the *projection matrix* and has the properties of being idempotent and symmetric. We can then take the non-background-like weighting vector $\mathbf{e}$ and project it onto a target spectrum $\mathbf{t}$. This produces the detector

$$T(\mathbf{x}) = \mathbf{t}^T\mathbf{P}_{\mathbf{B}}^{\perp}\mathbf{x} \tag{5}$$

which is a type of geometric matched filter. Most detectors (geometric or stochastic) are applied to atmospherically compensated imagery therefore $\mathbf{t}$ can come from a spectral library or simply be image derived. If the test pixel $\mathbf{x}$ is close to the background spanned by the endmembers, the orthogonal projection of $\mathbf{x}$ onto $\mathbf{B}$ will be small. Consequently, this produces a low test statistic value since $\mathbf{t}^T\mathbf{e}$ will be small as well. Therefore, we conclude that the pixel in question is background-like. Conversely, if the orthogonal projection of $\mathbf{x}$ onto $\mathbf{B}$ produces a large value, then we can say that the test pixel is not background and maybe target-like. Actual implementation usually requires a threshold or cut off value for the test statistic in order to judge whether image pixels are target or not.

The previously described detector was based on characterizing the background through use of geometry. There also exists families of detectors that are based on characterizing the background in terms of descriptive statistics, though we will not address them here. A *hybrid* detector, as described in this paper, may take

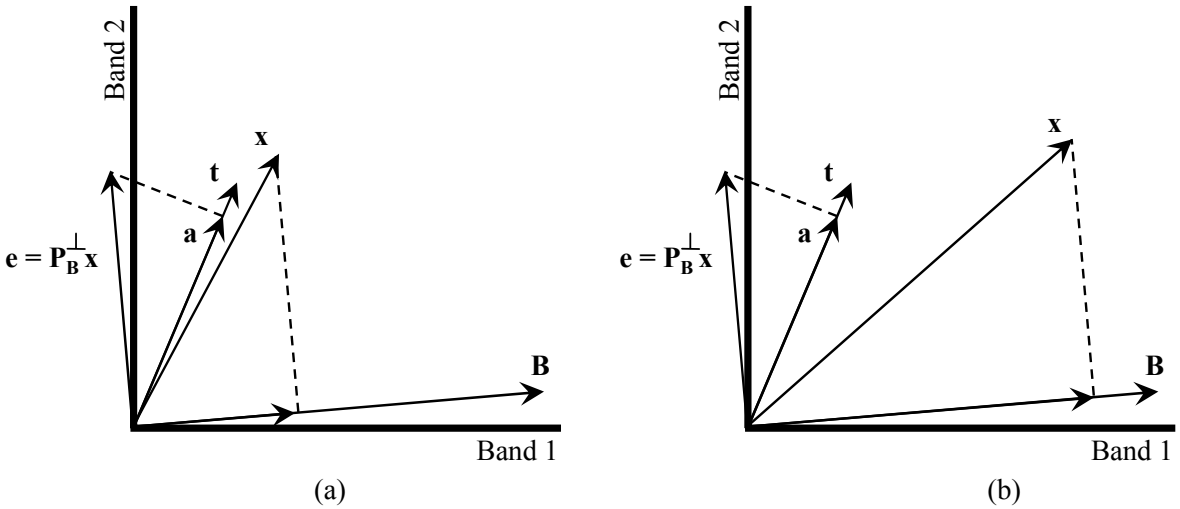

Figure 3. Illustration of a possible false positive using a matched filter. In (a) the image pixel $\mathbf{x}$ is close to the target and results in an abundance vector $\mathbf{a}$. In (b), however, it is questionable as to wether the image pixel is close to the target even though it produces the same abundance-like value as in (a).

advantage of both geometric and stochastic representations of the data. In addition, the detector may use data that is not derived from imagery, such as that created through physics based modeling. The hybrid detector we propose is based on geometry and includes the use of PBM. Additionally, the detector has an added metric (described in the next section) that takes advantage of target and background statistics.

2.4.1. Infeasibility Concept

The detector of Eq. (5) is a type of matched filter where we are weighting a target spectrum with an (orthogonal) projection of the test pixel with the background space. If the detector is normalized, we have what is often referred to as an *abundance*, where high abundance values mean the test pixel is very target-like. However, large abundances can also be generated by any spectral pixel that has a significant projection (*e.g.,* a bright or saturated pixel) thus producing false positives. Figure 3 illustrates this concept where we have two different pixels producing the same abundance *vector* $\mathbf{a}$. For this reason, we would like to use an additional *infeasibility* metric that helps us detect the presence of false positives relative to information about the target and background spaces. The infeasibility concept was originally introduced in the mixture tuned matched filter (MTMF).[10] Though there is no derivation of this approach in the current literature, it is believed to be based on a stochastic approach.[11] In this research we develop *geometric* version of this concept based on a geometric matched filter that uses PBM.

We start by estimating an abundance-like vector, for the pixel of interest, by projecting $\mathbf{e}$ onto $\mathbf{t}$ such that abundance vector $\mathbf{a}_1 = \mathbf{P}_t\mathbf{e} = \mathbf{P}_t\mathbf{P}_{\mathbf{B}}^{\perp}\mathbf{x}$, where $\mathbf{P}_t = \mathbf{t}\mathbf{t}^{\dagger}$ and $\mathbf{t}^{\dagger}$ is the pseudo-inverse of $\mathbf{t}$ defined as $\mathbf{t}^{\dagger} = (\mathbf{t}^T\mathbf{t})^{-1}\mathbf{t}^T$. The orthogonal projection of $\mathbf{x}$ onto the subspace orthogonal to $\mathbf{B}$ and subsequently onto $\mathbf{t}$ can be seen in Figure 4. This measure tells us how target-like the pixel is. We then wish to obtain a measure $\mathbf{d}$ of how un-target-like $\mathbf{x}$ is using an orthogonal projection onto the target vector (as seen in Figure 4). That is

$$\mathbf{d} = \mathbf{P}_t^{\perp}\mathbf{x} \tag{6}$$

where $\mathbf{P}_t^{\perp} = \mathbf{I} - \mathbf{t}\mathbf{t}^{\dagger}$ and $\mathbf{t}^{\dagger}$ is the pseudo-inverse of $\mathbf{t}$ as previously defined. Again, the target can come from a spectral library (assuming reflectance data) or be image derived. In this research we propose that the vector(s) of $\mathbf{t}$ come from a (radiance) target space created using physics based modeling. We now have a vector $\mathbf{d}$ that can be used to aid in the identification of pixels that have similar orthogonal projections onto the background but different projections onto the subspace orthogonal to the target space, as can be seen in Figure 4(b). Upon closer analysis of Figure 4(b) we notice that there are potentially a *family* of pixels (denoted by the dotted line connection the tip of $\mathbf{e}$ and $\mathbf{x}$) that can produce the same orthogonal projection onto the background $\mathbf{B}$, but

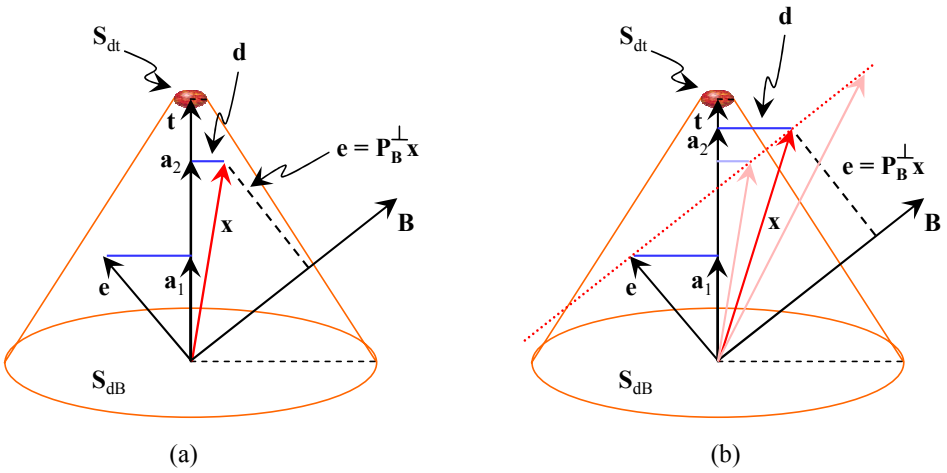

Figure 4. Illustration of infeasibility concept as hyper-cones. (a) The projection of a pixel $\mathbf{x}$ onto the background $\mathbf{B}$ produces vector $\mathbf{e}$ which is then projected onto target $\mathbf{t}$ to produce and abundance-like vector $\mathbf{a}_1$. Additionally, we can generate an orthogonal target-like vector $\mathbf{d}$. (b) Shows that we can get the same abundance vector for a "family" of possible pixels, all of which, however, have different $\mathbf{d}$ values, which we can take advantage of in generating an infeasibility metric.

with different $\mathbf{d}$ values. The question now becomes that of where to set a threshold. What we propose in this research is to establish a measure based on the joint statistics of target and background spaces.

If the background has covariance $\mathbf{\Sigma}_B$ (or diagonal matrix $\mathbf{\Lambda}_B$ if working in a de-correlated space) then we can transform it into a space such that it is orthogonal to the target space using our orthogonal target space projection operator. That is:

$$\mathbf{S}_{dB} = \mathbf{P}_t^{\perp} \mathbf{\Sigma}_B \mathbf{P}_t^{\perp}. \tag{7}$$

Because we are using the physics based modeling approach, which generates a *target space*, we assume its variability in this subspace orthogonal to the target is described by $\mathbf{\Sigma}_t$. Similarly, we can transform the target covariance as:

$$\mathbf{S}_{dt} = \mathbf{P}_t^{\perp} \mathbf{\Sigma}_t \mathbf{P}_t^{\perp}. \tag{8}$$

These transformed distributions are illustrated at the top and bottom of Figure 4 as 3 dimensional ellipses. In this case, we can imagine that the orthogonal target / background space combination forms a hyper-dimensional *cone*, the size of which is determine by the variance mixture between the target and background. We can create this mixture by modulating the transformed target and background covariances by the abundance-like term as

$$\mathbf{S}_d(a) = a^2 \mathbf{S}_{dt} + (1-a)^2 \mathbf{S}_{dB} \tag{9}$$

where the scalar $a = ||\mathbf{a}_1||/||\mathbf{P}_t \mathbf{P}_{\mathbf{B}}^{\perp} \mathbf{t}||$. This covariance mixture (based on target and background data) enables us to standardize our orthogonal un-target-like measure, $\mathbf{d}$ as

$$INF = \mathbf{d}^T \mathbf{S}_d(a)^{-1} \mathbf{d}. \tag{10}$$

where INF is a statistical measure, called the *infeasibility*, of how far a pixel is from the expected target/background mixture. We would like the infeasibility metric to produce large values, corresponding to false positives, when both $\mathbf{d}$ and our measure of abundance are large. Low abundance targets might have relatively large $\mathbf{d}$ values that would be scaled to smaller INF reflecting the larger variance in the $\mathbf{d}$ space for low abundance targets (*i.e.,* higher mixture of background). The metric is applied to each pixel and produces a map of infeasibility scores. We can then analyze our detects and compare them to infeasibility scores to determine if any detects are suspect to being false alarms.

3. RESULTS

3.1. Creation of Target and Background Spaces

3.1.1. Target Space

Target spaces were created using the physics based model of Eq. (1) in conjunction with MODTRAN. The reflectance used was that of a panel found in the HYDICE Forest Radiance I (FRI) imagery. This target was measured with a hand held spectrometer around the time of the FRI acquisition, resampled according to Eq. (2) and used in Eq. (1) to generate sensor reaching spectra.

For this simple study, 5 different visibility values were used along with 4 elevations, 5 scalings of the vertical water vapor, and 3 different target orientation angles for a total of 320 sensor reaching radiance vectors. These parameters are summarized in Table 1. Additionally, the model atmosphere used was midlatitude summer with a rural extinction profile. The parameters were chosen based on some *a priori* knowledge about the FR1 acquisition. For example, the time of day for the selected FR1 image was known to be 9:10 EDT. This generated a Sun zenith angle of 60 degrees. Therefore, the target angle variations in Table 1 correspond to a rotation or tilting of the target away (-) or toward (+) the Sun. For example, if the target is simply tilted -10 degrees away from the Sun, for the given TOD, this would result in a 32% reduction in illumination.

Table 1. Parameters varied in creating target space.

Visibility [km]	10, 15, 20, 40
Elevation [km]	1.0, 1.2, 1.4, 1.6
WV Scale Factor	0.3, 0.5, 0.7, 1.5, 2.0
Target Angle [deg]	-10, -5, +5

The target space with out any tilting or rotational effects of the target can be seen in Figure 5(a). When we factor in illumination angle effects we get that of Figure 5(b). A simple visual check was performed to see if the image target pixels for the panel (in radiance space) were encompassed by the target space. This is illustrated in Figure 5(b) where we see that all the image target pixels for the target of interest, fall with in the set of physically generated target vectors. If desired, the target space can be reduced to a set of basis vectors spanning the space using the maximum distance method. Additionally, methods based on variance exploitation, such as the singular value decomposition (SVD), can also be used as a means of dimensionality reduction. For this study, we simply used the mean vector of the space.

3.1.2. Background Space

Background spaces were described with endmembers found using the MaxD algorithm. Endmembers were generated based on a 100×100 pixel subset of the Forest Radiance I image. The subset contained classes of grass, trees, road, and 12 target panels (full and subpixel) of varying size representing 4 different materials (3 panels for each material). Prior to endmember determination, the background data was augmented with the target space radiance vectors. Simply running an automated endmember routine, such as MaxD, may result in finding endmembers that are actually targets of interest. These target endmembers would then be included in the description of the background space. If an orthogonal-type projection operator is then used, actual targets will get suppressed along with the background since they are part of the background description. This "masking" of the targets with the target space forces the endmember routine to select target endmembers from the target space and not the target image pixels. Since we know which vectors went into the augmentation, we can simply remove them after the algorithm has run, in the event that they are found. To further reduce the complexities of hyper-dimensional space, we performed the endmember selection process in a principal components (PC) space. To gain better separation of noise and signal, a noise adjusted principal components (NAPC) space could be employed, where the noise in the rotated space is of unit variance. A set of 15 endmembers were selected to characterize the background based on previous endmember selection studies.[12, 13]

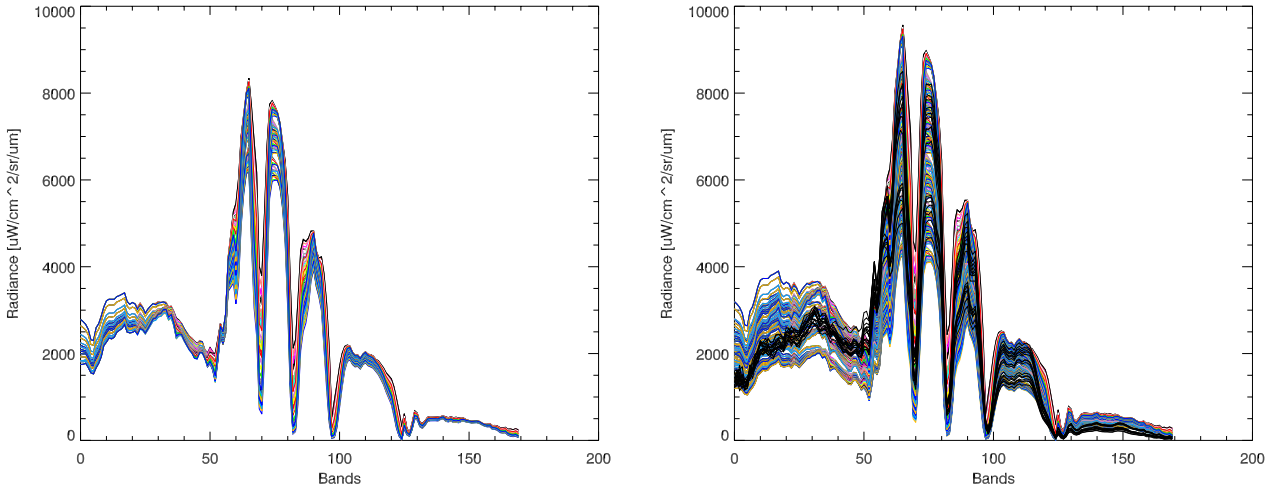

Figure 5. (a) Eighty vector target space with out any effects of magnitude scaling due to sun-target-sensor angle (*i.e.,* projected area cosine falloff) and (b) expanded 320 vector target space including 3 illumination or rotation angles. Overlayed in (b) are all the full radiance image pixels from the panel target found in the data set. Some bands were eliminated due to poor signal to noise caused by water vapor absorption, for example. This left a total of 170 valid bands (out of 210).

3.2. Application of Detector and Infeasibility Metric

The first part of the algorithm evaluation was to determine if the un-target-like projection operator $\mathbf{P}_{\mathbf{t}}^{\perp}$ behaved as expected when integrated with a target space generated using physics based modeling. This was accomplished by formulating the (orthogonal) projection operator with a mean target vector $\boldsymbol{\mu_t}$ from our physically modeled target space. We then applied the operator to a target and background pixel (see Figure 6). Figure 6(a) illustrates the amount of suppression (dotted line) set forth when we operate on a typical target pixel. Over plotted is the actual target pixel spectrum. When applied to a background pixel, however, we see that $\mathbf{d}$ is much larger and un-target-like, as seen in Figure 6(b). Again, over plotted is a typical background pixel spectrum. This tells us that the projection operator is behaving as expected and that vectors in the physics based modeled target space resemble target spectra in the image.

We then applied our un-target-like orthogonal projection operator to all 10,000 image pixels. This can be seen in Figure 7(a) where small $\mathbf{d}$ values are associated with target pixels. Large values, however, would equate to highly un-target-like pixels or anomalies. Finally, we looked at the relationship between the abundance-like term (*i.e.,* how target-like a pixel is) and the un-target-like term. This can be seen in Figure 7(b). Here we see pixels with small $\mathbf{d}$ values and relatively large abundances. These image pixels correspond to targets. Additionally, we see a small cluster of pixels with very low abundance but large $\mathbf{d}$ values. That is, they do not look like either background or target and are thus deemed anomalous.

This level of testing demonstrates that the orthogonal projection operator behaves as expected. Furthermore, it tells us that the use of physics based modeling in this scheme is possible. Ultimately, however, we wish to incorporate the statistics of the target and background spaces into our earlier developed infeasibility metric. To date, we have yet to test this metric on known false positives. This infeasibility testing is our next step in the development of this approach to detection.

4. CONCLUSIONS

This research demonstrated the current status of RIT's implementation of the invariant method in generating physics based target spaces. We also successfully illustrated how physics based modeling can be integrated into an

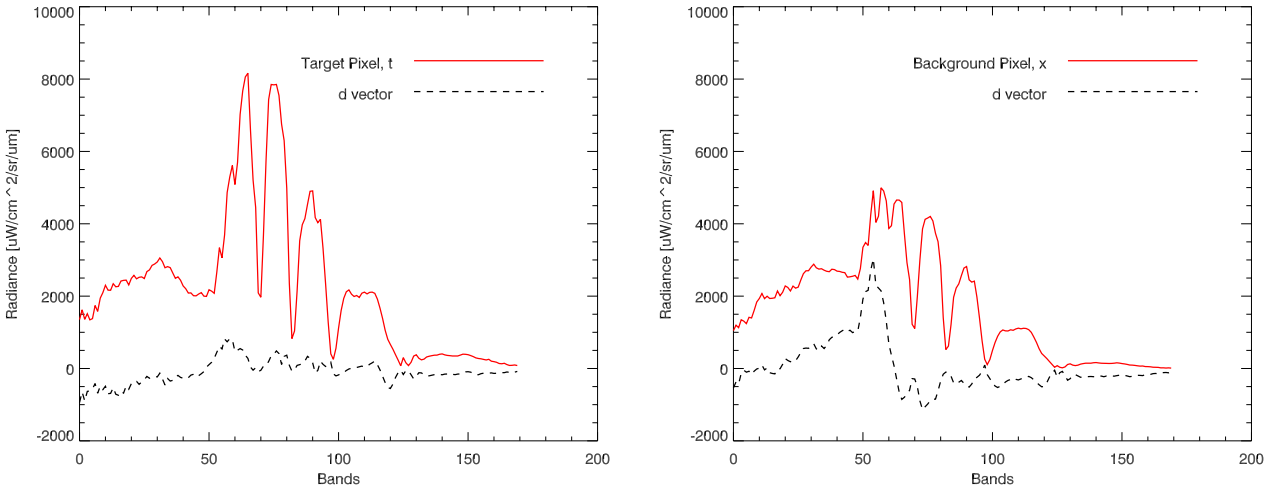

(a) (b)

Figure 6. Testing of $\mathbf{P}_{\mathbf{t}}^{\perp}$ operator, using physics based modeling, on (a) target and (b) background pixels.

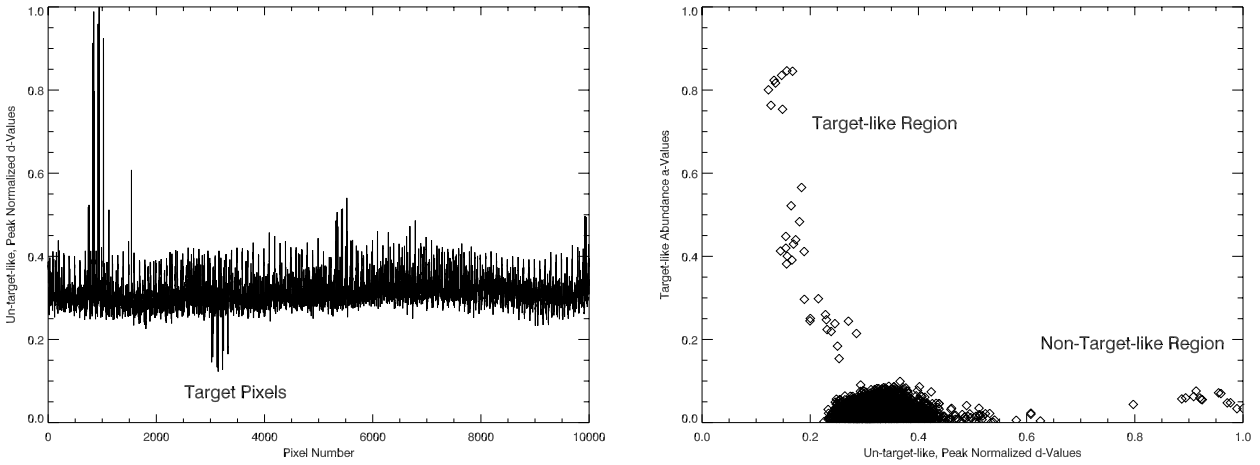

(a) (b)

Figure 7. (a) Magnitude of the orthogonal un-target-like projection operator **d**, constructed from the physics based target space, applied to all 10,000 image pixels. We can see that target pixels stand out using this operator. (b) Magnitude plot of target-like and un-target-like behavior of pixels using our previously defined values of a and **d**.

orthogonal projection operator to determine un-target-like characteristics of image pixels. This result, together with a matched filter that incorporates background information, was used to separate target, background, and anomalous pixels. Finally we developed a geometric infeasibility metric that can be used to identify pixels related to potential false positives. Collectively, these results form the basis of a new hybrid detection scheme.

This concept is still in its infancy and is the subject of ongoing testing and evaluation. In the future we would like to address the issue of working in a reduced dimension space via principal components space (PC) or noise adjusted principal components (NAPC). Additionally, work on the detector itself includes a false positive test case along with analysis of normality assumptions and the impact a target pixel has on the background covariance estimation. We plan to apply the detector to other image data sets and targets.

ACKNOWLEDGMENTS

The author would like to thank David Messinger and Professor John Kerekes for suggestions regarding this paper. This work was funded under the Office of Naval Research Multi-disciplinary University Research Initiative "Model-based Hyperspectral Exploitation Algorithm Development" #N00014-01-1-0867.

REFERENCES

1. G. Healey and D. Slater, "Models and methods for automated material identification in hyperspectral imagery acquired under unknown illumination and atmospheric conditions," *IEEE Transactions on Geoscience and Remote Sensing* **37**, pp. 2706–2717, November 1999.
2. J. Schott, *Remote Sensing: The Imaging Chain Approach*, Oxford University Press, New York, 1997.
3. A. Berk, L. Bernstein, and D. Robertson, "MODTRAN: A moderate resolution model for LOWTRAN 7," Technical Report GL-TR-89-0122, Air Force Geophysics Laboratory, Hanscom AFB, MA, 1988.
4. D. Slater and G. Healey, "Physics-based model acquisition and identification of airborne spectral images," in *Eighth IEEE International Conference on Computer Vision*, **2**, pp. 257–262, IEEE, July 2001.
5. M. King, W. Menzel, P. Grant, J. Myers, S. Arnold, G.T. Platnick, L. Gumley, S. Tsay, C. Moeller, M. Fitzgerald, K. Brown, and F. Osterwisch, "Airborne scanning spectrometer for remote sensing of cloud, aerosol, water vapor and surface properties," *J. Atmos. Oceanic Technol.* **13**, pp. 777–794, 1996.
6. D. Schlapfer, C. Borel, J. Keller, and K. Itten, "Atmospheric precorrected differential absorption technique to retrieve columnar water vapor," *Remote Sensing of Environment* **65**(3), pp. 353–366, 1998.
7. K. Hirsch, L. Balick, C. Borel, and M. P., "A comparison of four methods for determinging precipitable water vapor conten from multi-spectral data," in *Proc. SPIE, Algorithms and Technologies for Multispectral, Hyperspectra, and Ultraspectral Imagery VII*, S. S. Shen and M. R. Descour, eds., **4381**, pp. 417 – 428, SPIE, (Orlando, Fla), April 2001.
8. K. Lee, *A sub-pixel scale target detection algorithm for hyperspectral imagery.* PhD dissertation, Rochester Institute of Technology, 54 Lomb Memorial Drive, Rochester, NY, 2003.
9. J. Schott, K. Lee, R. Raqueno, G. Hoffmann, and G. Healey, "A sub-pixel target detection technique based on the invariance approach." To be published, 2004.
10. J. W. Boardman, "Leveraging the high dimensionality of AVIRIS data for improved sub-pixel target unmixing and rejection of false positives: mixture tuned matched filtering," in *Summaries of the Seventh Annual JPL Airborne Geoscience Workshop*, R. O. Green, ed., *JPL Publication 97-21* **1**, p. 55, (Pasadena, California), January 1998.
11. "Personal conversation between John R. Schott and Joseph W. Boardman," 2004.
12. P. Bajorski, E. Ientilucci, and J. Schott, "Comparison of basis-vector selection methods for target and background subspace as applied to subpixel target detection," in *Proc. SPIE, Algorithms and Technologies for Multispectral, Hyperspectra, and Ultraspectral Imagery X*, S. S. Shen and P. E. Lewis, eds., **5425**, pp. 97–108, SPIE, (Orlando, Fla), April 2004.
13. P. Bajorski and E. Ientilucci, "Geometric basis-vector selection methods and subpixel target detection as applied to hyperspectral imagery," in *IEEE International Geoscience and Remote Sensing Symposium (IGARSS)*, (Anchorage, Alaska), September 2004.